Available online at www.sciencedirect.com
SCIENCE DIRECT®
Applied Surface Science xxx (2005) xxx–xxx
applied surface science
www.elsevier.com/locate/apsusc

Synergetic effect between ion energy and sample temperature in the formation of distinct dot pattern on Si(1 1 0) by ion-sputter erosion

Wei-Qing Li [a], Le-Jun Qi [a], Xinju Yang [b,*], Li Ling [a], Wen-Bin Fan [a], You-Yuan Zhao [a], Ming Lu [a,*]

[a] *Department of Optical Science and Engineering, State Key Laboratory for Advanced Photonic Materials and Devices, Fudan University, Shanghai 200433, China*
[b] *Surface Physics Laboratory, Fudan University, Shanghai 200433, China*

Received 15 July 2005; received in revised form 12 September 2005; accepted 12 September 2005

Abstract

We observed a synergetic effect between ion energy and sample temperature in the formation of distinct dot pattern on Si(1 1 0) by Ar^+ ion sputtering. The ion flux was 20 $\mu A/cm^2$, a value smaller than those used in preceding reports by one or two orders of magnitude. In experiments, the ion energy was from 1 to 5 keV, and the temperature from room temperature to 800 °C. A phase diagram indicating the ranges of ion energy and temperature within which distinct dot patterns can be achieved has been obtained. Data analyses and simulation results reveal that the synergetic effect is consistent with the effect of the Ehrlich–Schwoebel step-edge barrier, rather than the Bradley–Harper model.

PACS: 68.35.Bs; 68.37.Ps; 68.49.Sf

Keywords: Silicon; Surface structure, morphology, roughening and topography; Ion bombardment; Atomic force microscopy

1. Introduction

Nanostructuring of silicon, the mainstream material of modern microelectronic industry, has received much attention due to its potential application in developing Si light sources [1]. Si nanomaterials such as porous Si, Si nanocrystal-doped dielectrics and Si quantum dots have been developed in self-organized manners by various techniques such as acid etching, ion implantation, reactive evaporation, chemical vapor deposition and molecular beam epitaxy [1–8]. In the past few years, the technique of ion-sputter erosion that is normally used for sample milling, depth

* Corresponding authors. Tel.: +86 21 55664059/65642177; fax: +86 21 65641344.
E-mail addresses: xjyang@fudan.ac.cn (X. Yang), minglu@fudan.ac.cn (M. Lu).

0169-4332/$ – see front matter © 2005 Elsevier B.V. All rights reserved.
doi:10.1016/j.apsusc.2005.09.019

profiling and mass analysis has aroused new interest as a method of producing nanodot arrays on solid surfaces [9–22]. As compared to other self-organization methods, ion-sputter erosion is able to produce well-ordered and spatially dense nanodots, and to easily control the size of nanodots by simply changing sputtering parameters such as ion energy, ion dose, ion flux and sample temperature. Up to now, the Bradley–Harper (BH) theory and its revised versions [23–26] based on the concept of surface–curvature dependent sputtering yield, have found applications in the nanostructuring of semiconductor single crystals, especially when the ion flux is sufficiently high [9–14,17–20]. However, for the nanostructuring of metal single crystals [15,17], a model stemming from the Ehrlich–Schwoebel (ES) step-edge barrier [17,27,28] is active. So far a complete understanding of this technique in nanodot formation has not been realized, and new experimental results continuously emerge, which challenges the current theories and enriches our understanding of this novel nanostructuring process.

In this paper, we report a synergetic effect between ion energy (E) and sample temperature (T) in producing distinct nanodot patterns on Si(1 1 0), which was found during our investigation of the nanodot formation by normal-incident Ar^+ ion sputtering with ion flux of 20 $\mu A/cm^2$ as a function of E and T. A phase diagram was constructed, exhibiting the ranges of E and T for the creation of distinct dot patterns. The experimental results cannot be explained by the BH theory, but could be well understood with the help of a dynamic continuum equation [25] that emphasizes the ES effect.

2. Experiments

Si(1 1 0) wafers (p-type, 1–10 Ω cm) were used. After supersonically cleaned in acetone and alcohol in sequence and dried in air, the sample was transferred into the vacuum chamber of a home-built ion sputtering system. The normal-incident Ar^+ ion sputtering was conducted with a Perkin-Elmer sputtering gun (model 04-303). The distance between the outlet of ion gun and the sample was 13 cm, and ion beam spot size was ~5 mm in diameter. The pressure of argon in the ionization chamber of ion gun was kept at 25 mPa. Prior to sputtering, the ion flux was measured with a Faraday cup located above the sample holder. The ion flux was chosen to be 20 $\mu A/cm^2$ and ion energy ranged from 1 to 5 keV. The base pressure of the chamber was better than 5×10^{-7} Pa, and during sputtering, the pressure rose to $\sim 5 \times 10^{-5}$ Pa due to the backfilling of argon with purity of 99.999%. Sample heating was accomplished through biased electron beam bombardment at the backside of the sample. The temperature was measured with a calibrated thermocouple, which ranged from room temperature (RT, ~25 °C) to 800 °C. Ar^+ dose was kept constant as 5×10^{17} ions/cm^2. Surface morphology was measured ex situ with an ambient atomic force microscopy (AFM), model Solver P47 of NT-MDT, at RT in contact mode.

3. Results

In Fig. 1, six typical AFM images for Si(1 1 0) surfaces after different heating and ion sputtering treatments are presented. It is seen from Fig. 1a that when heating the sample in vacuum at 800 °C for ~1 h, the same time needed to reach the required dose of 5×10^{17} ions/cm^2 for ion sputtering, no distinct dot pattern forms. Either, if the Si(1 1 0) surface is sputtered at RT with ion energy of 1.5 keV, no distinct dot pattern is observed (Fig. 1b), but the surface is featured by diffused small dots and holes with a low surface roughness which will be illustrated in Fig. 2a. However, when heating and sputtering the sample *simultaneously*, a distinct dot pattern appears (Fig. 1c) and the surface roughness becomes high (Fig. 2b). This indicates a synergetic effect between ion energy (E) and sample temperature (T) in producing distinct nanodot patterns on Si(1 1 0). Fig. 1d and e gives the images of Si(1 1 0) after ion sputtering with $E = 1.5$ keV at $T = 600$ °C and $T = 400$ °C, respectively. It is clear that for $E = 1.5$ keV, the lowest temperature (or T_0) required to create distinct dot pattern according to the synergetic effect must fall in the range of $400\ °C < T_0 \leq 600\ °C$. We later on narrowed this range to be $550\ °C < T_0 \leq 600\ °C$ by further experiments as will be shown in Fig. 3. The surface roughness defined as the root of mean square of the difference between the height at any surface position and the average height has been plotted against temperature in Fig. 2a for $E = 1.5$ keV. By

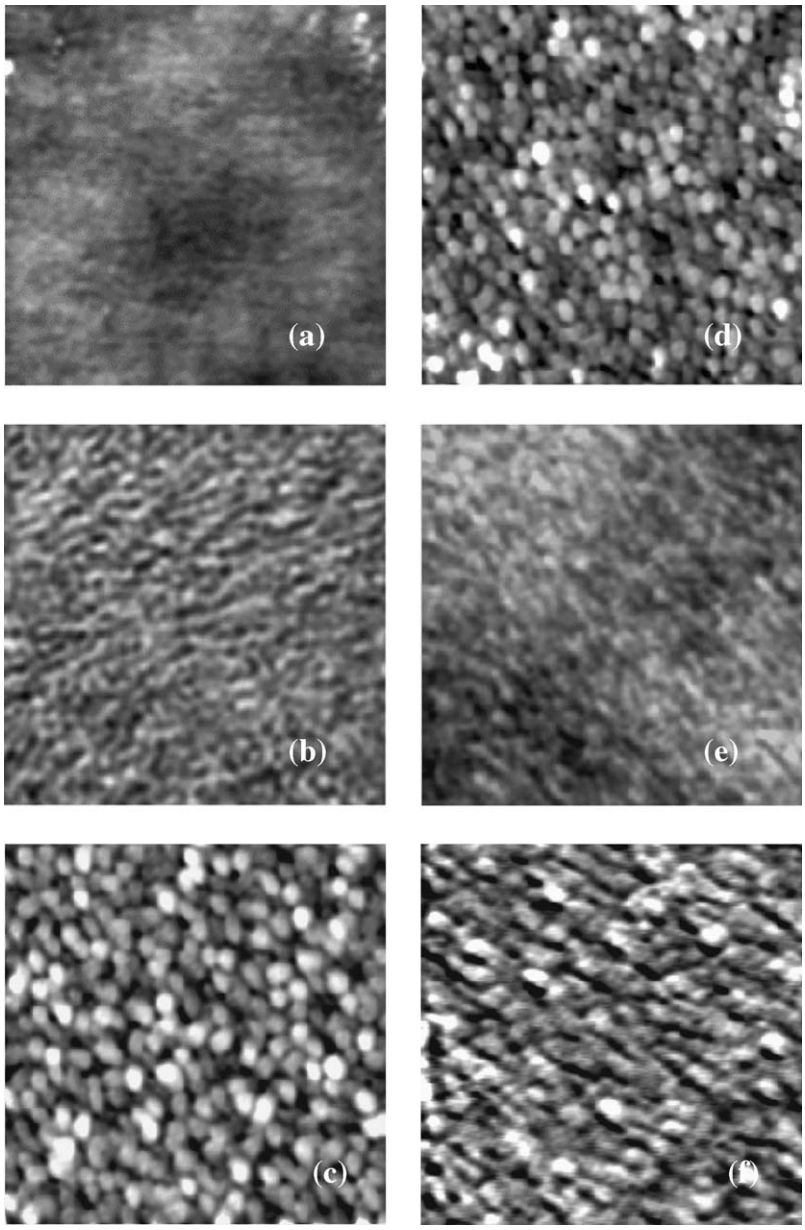

Fig. 1. AFM images of the sputtered surfaces of: (a) $T = 800\ ^{\circ}C$, no ion sputtering; (b) $T = RT$, $E = 1.5$ keV; (c) $T = 800\ ^{\circ}C$, $E = 1.5$ keV; (d) $T = 600\ ^{\circ}C$, $E = 1.5$ keV; (e) $T = 400\ ^{\circ}C$, $E = 1.5$ keV; (f) $T = 400\ ^{\circ}C$, $E = 5$ keV. The image size is 800 nm $\times$ 800 nm. The ion flux = 20 $\mu A/cm^2$.

comparison with Figs. 1c–e and 2a, it is seen that the appearance of distinct dot pattern coincides with the abrupt increase in the surface roughness. This is also true for the case of other ion energies. Hence, this abrupt increase in surface roughness can be regarded as a criterion for the formation of distinct dot pattern.

In the meantime, we have also performed the ion energy dependence study of the dot pattern formation. It has been reported that at $T = 800\ ^{\circ}C$, both the shape and size of dots in the distinct dot pattern change with the increasing E [21]. But in this paper, we only focus on the synergetic effect. It is found that for the higher

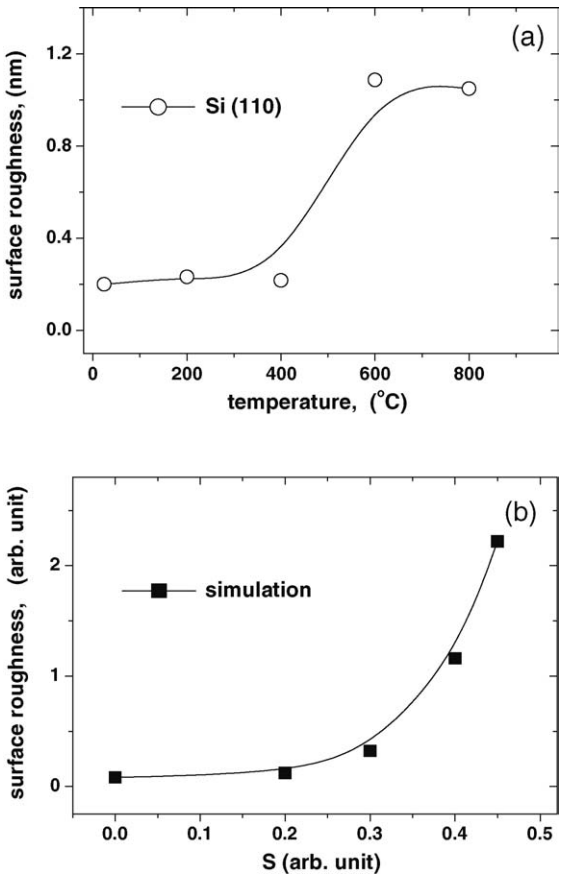

Fig. 2. (a) Surface roughness vs. sample temperature; $E = 1.5$ keV. (b) Calculated surface roughness vs. S, which increases with the increasing T before the critical temperature.

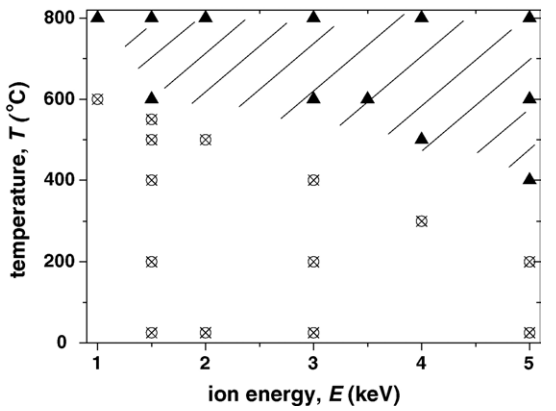

Fig. 3. Phase diagram of temperature (T) and ion energy (E) in the ranges of RT, 800 °C and 1–5 keV. The hatched part denotes the regime for the distinct dot pattern.

E, T_0 becomes lower; for example, in Fig. 1f where $E = 5$ keV and $T = 400^\circ$, it is seen that as compared to Fig. 1e where $E = 1.5$ keV and $T = 400$ °C, a dot pattern emerges. A number of E–T pairs have been tried to see if distinct dot pattern can be created, and based on these data, a phase diagram was constructed as shown in Fig. 3 within the experimental ranges of temperature (RT, 800 °C) and ion energy (1–5 keV). The hatched part denotes the E–T regime for the formation of distinct dot pattern, while the rest one indicates that of diffused small dots and holes. A distinct separation between these two regimes is difficult, since around the ''border'' region, surface morphology represents a mixture of both regimes.

4. Discussion

At present, a dynamic continuum equation, namely, the noisy Kuramoto–Sivashinsky (KS) equation [17,25], has been widely accepted and employed to describe the nanostructuring process by ion sputtering. The KS equation contains both the BH and ES models, which reads:

$$\frac{\partial h}{\partial t} = \sum_{\vec{n}} \left\{ -(\nu_{\vec{n}} + S_{\vec{n}}) \frac{\partial^2 h}{\partial \vec{n}^2} + \left(\frac{\partial h}{\partial \vec{n}} \right)^2 \frac{\lambda_{\vec{n}}}{2} - \frac{D_{\vec{n}} \partial^4 h}{\partial \vec{n}^4} \right\} + \eta(x, y, t), \quad (1)$$

where $h(x, y, t)$ is the height of a position (x, y) on surface at time of t; $\vec{n}$ represents crystallographic directions; $-(\nu_{\vec{n}} + S_{\vec{n}})$ is the effective surface tension, where $\nu_{\vec{n}}$ is generated by ion sputtering, and normally temperature-independent and greater than 0; $S_{\vec{n}} \partial^2 h / \partial \vec{n}^2$ represents the ES diffusion with $S_{\vec{n}} \geq 0$ and sensitive to the temperature. The second term includes non-linear effect with $\lambda_{\vec{n}}$ being the tilt-dependent erosion rate, and $D_{\vec{n}} \partial^4 h / \partial \vec{n}^4$ takes into account the thermal and/or ion-induced diffusions with $D_{\vec{n}} > 0$. The last term reflects a stochastic noise. If the ES diffusion is neglected, i.e. $S_{\vec{n}} = 0$, Eq. (1) is reduced to the pure BH model. On the other hand, if $S_{\vec{n}}$ is comparable with $\nu_{\vec{n}}$, and the effective surface tension becomes strongly temperature-dependent, then the ES effect is mainly at work.

The pure BH model that is normally accepted as good for semiconductors [17] is unable to explain the results of Fig. 3. For instance, for a fixed E, increasing

T should always reduce the surface roughness [11,14,22] as the effective surface tension $\nu_{\vec{n}}$ that is responsible for surface instability is nearly temperature-independent, while the surface diffusion, or $D_{\vec{n}}$, that is responsible for surface smoothing, increases dramatically. This is not the observation in this work (Figs. 2a and 3). In fact, we recently identified [22] that for sufficiently low ion flux such as 20 μA/cm^2 used here, the ES effect is strongly involved in the nanostructuring of Si single crystals. This is not unrealistic. For instance, de Souza et al. [29] pointed out that at temperatures above as low as about -120 °C, the recombination of vacancies and self-interstitials of Si, created by the collision events in crystalline Si, can already be facilitated by the increasing of their mobility, a process called dynamic annealing. When the ion flux is sufficiently low and the sample temperature is sufficiently high, the dynamic annealing process may become so effective that a full amorphization of Si by ion implantation is blocked. In this case, the sputtered surface is not fully amorphized, and remains parts of its crystalinity, which allows the ES effect available. Hence, the synergetic effect is related to the ES diffusion-induced surface instability.

The ES diffusivity, or $S_{\vec{n}}$, is proportional to the rebounding probability at step edges as well as the step-climbing and terrace diffusion probabilities [21], i.e.

$$S_{\vec{n}} \propto \left(1 - \mathrm{e}^{-E_{\mathrm{ES}}/k_{\mathrm{B}}T}\right) \mathrm{e}^{-(E_0+E_1)/k_{\mathrm{B}}T}\big|_{\vec{n}}, \qquad (2)$$

where E_{ES} is the ES step-edge barrier, and E_0 and E_1 are the step-climbing barrier and the terrace diffusion activation energy, respectively. k_{B} is Boltzmann's constant. Eq. (2) indicates that the ES diffusivity versus T follows a bell-shape like relationship, that is, before a critical temperature which corresponds to the maximum of $S_{\vec{n}}$, the effective surface tension increases with increasing T if the ES effect is dominant, and beyond that temperature, the surface tension falls down. This leads to the surface roughness evolution with T as shown in Fig. 2a. Similar bell-shape like relationship has also been found during deposition of Si atoms onto Si(1 0 0) by Schelling et al. [30], only in their case the temperature corresponding to the maximal peak-to-valley height, the critical temperature, is lower than that shown in Fig. 2a by ~100–200 °C depending on the deposition rate. These surface roughness versus temperature relationships for deposition and negative deposition (i.e. ion sputtering) processes have also been observed on Ag(1 0 0) by Costantini et al. [31], with the critical temperature of deposition process being ~100 °C lower than that of negative deposition one as well. Considering that the critical temperatures for the case of Si(1 0 0) are ~300 °C lower than those of Ag(1 0 0) for the processes of both deposition and negative deposition, the ES barriers on Ag(1 0 0) should be smaller than those on Si(1 0 0).

We conducted temperature-dependent simulation of surface morphology evolution based on Eq. (1) with the help of Eq. (2). The algorithm used in Ref. [23]. was adopted with $\nu_{\vec{n}}$ being a constant and $S_{\vec{n}}$ increasing with the increasing T. For brevity, $D_{\vec{n}}$ was taken as a constant, which does not alter the general conclusion [21]. Four typical images of simulated results are given in Fig. 4, and in Fig. 2b their corresponding surface roughness data are presented. The simulation results show that when the surface roughness starts to increase quickly, a distinct dot pattern emerges, which agrees with the experimental results and confirms the availability of the ES effect.

With the above conclusions, the synergetic effect can then be readily explained. When the ES effect is mainly in operation, it is the ES diffusions of adatoms or/and vacancies that result in the surface instability. It is thus understood that heating the sample alone cannot form the dot pattern (Fig. 1a), since there is no provision of adatoms or/and vacancies due to the ion sputtering [31] for the ES diffusion. However, when the temperature is not high enough, the ES diffusion is too inefficient to cause a significant surface instability, accordingly, the dot pattern is still unavailable (Fig. 1b). Only when the adatoms or/and vacancies are provided, i.e. the surface under ion sputtering, and in the meanwhile, the temperature is high enough ($\geq T_0$) to promote strong ES diffusions, can the distinct dot pattern be expected. That is the physics underlying the synergetic effect. At the higher E, more energies are transferred to adatoms or/and vacancies, which has a similar effect of the increasing temperature on the ES diffusions of the two species, provided the surface still keeps sufficient parts of its crystalinity. Hence, the high energy helps enhance the ES diffusion, thus reducing T_0 for the formation of the distinct dot pattern.

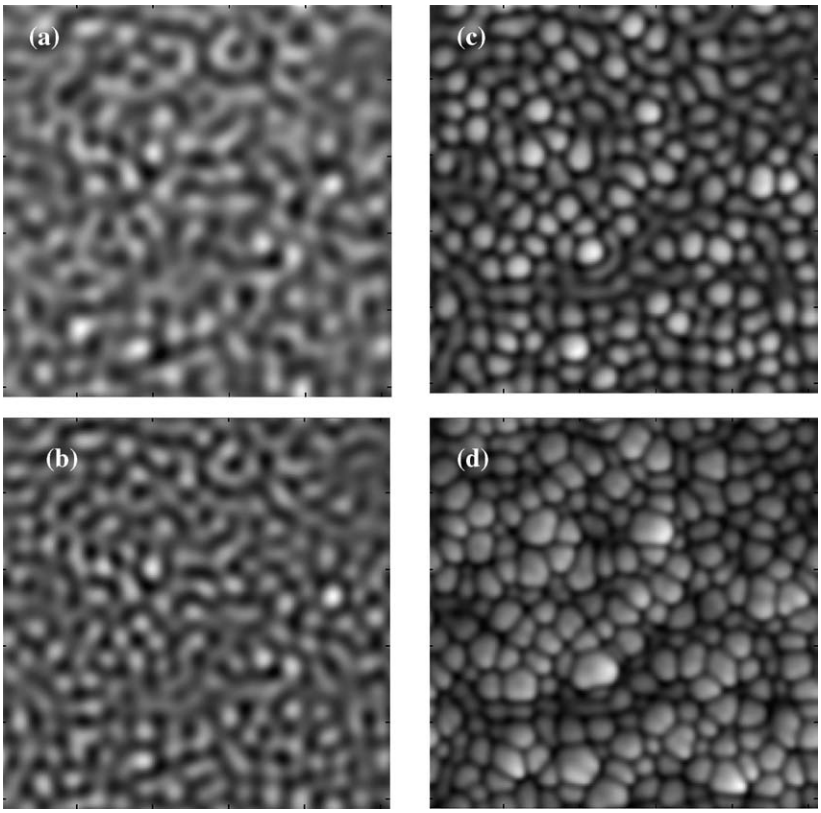

Fig. 4. Images from simulation calculations. $\lambda_{\vec{n}} = 1$, $D_{\vec{n}} = 2$, $\nu_{\vec{n}} = 0.2$ and the total time = 10^4, for: (a)$S_{\vec{n}} = 0.2$, (b) $S_{\vec{n}} = 0.3$, (c) $S_{\vec{n}} = 0.4$ and (d) $S_{\vec{n}} = 0.45$.

It should be pointed out, however, that the phase diagram does not mean that if the temperature is further increased, the minimum ion energy can be further reduced to create a distinct dot pattern. This is because for the temperature much higher than the critical temperature, the adatoms or/and vacancies may overcome the step-edge barriers, making the surface instability induced by ES diffusion depressed. Hence, the surface roughness is reduced and the distinct dot pattern becomes blurred. This is the situation observed for Ag(1 1 0) and Ag(1 0 0) [17]. Similarly, the phase diagram either does not indicate that if the ion energy is further increased, the T_0 can be further reduced to have a distinct dot pattern. The reason is similar to the case of temperature increase, considering that the ion energy effect is similar to that of temperature. Only for the case of ion energy, it is a bit more complicated in that the increasing E does not only promote the surface diffusion, but also increases the defect production rate [32], which tends to make the sample less crystalline and the ES effect less effective. However, it is noticed that under the conditions of RT and 5 keV ion sputtering, the distinct dot pattern cannot be developed on Si(1 1 0) surface (Fig. 3), indicating that the surface is not fully amorphized, and the surface morphology evolution is still mainly controlled by the ES effect. This is possible since the increasing ion energy promotes the mobility of vacancies and self-interstitials and facilitates the dynamic annealing when generating more defects at the meantime. Thus, the above discussion regarding the role of ion energy within the ion energy range in this work is reasonable.

5. Conclusions

The synergetic effect between ion energy and sample temperature in the formation of distinct dot pattern on Si(1 1 0) by ion sputtering has been reported.

A phase diagram indicating the ranges of ion energy and temperature within which distinct dot pattern can be achieved has been constructed. Within the experimental ranges of ion energy and sample temperature and for the ion flux of 20 $\mu A/cm^2$ used in this work, the synergetic effect is consistent with the Ehrlich–Schwoebel model.

Acknowledgements

This work was supported by the NSFC under grant No. 10374016, and the Science and Technology Commission of Shanghai under the grant of Key Project, No. 03DJ14001.

References

[1] For instance
G. Amato, C. Delerue, M.-J. von Bardeleben (Eds.), Structural and Optical Properties of Porous Silicon Nanostructures, vol. 5, Gordon and Breach, Amsterdam, 1997;
O. Bisi, S.U. Campisano, L. Pavesi, F. Priolo (Eds.), Silicon Based Microphotonics: From Basic to Applications, IOS Press, Amsterdam, 1999.
[2] L.T. Canham, Appl. Phys. Lett. 57 (1990) 1046.
[3] L. Pavesi, L.D. Negro, C. Mazzoleni, G. Franzo, J.P. Prolo, Nature 408 (2000) 440.
[4] S. Cheylan, R.G. Elliman, Appl. Phys. Lett. 78 (2001) 1225.
[5] N.-M. Park, T.-S. Kim, S.-J. Park, Appl. Phys. Lett. 78 (2001) 2575.
[6] M. Zacharias, J. Heitmann, R. Scholz, U. Kahler, M. Schmidt, J. Bläsing, Appl. Phys. Lett. 80 (2002) 661.
[7] Y.C. Fang, Z.J. Zhang, Z.Q. Xie, Y.Y. Zhao, M. Lu, Appl. Phys. Lett. 86 (2005) 191919.
[8] F. Xue, J. Qin, J. Cui, Y.L. Fan, Z.M. Jiang, X.J. Yang, Surf. Sci. 592 (2005) 65.
[9] S. Facsko, T. Dekorsy, C. Koerdt, C. Trappe, H. Kurz, A. Vogt, H.L. Hartnagel, Science 285 (1999) 1551.
[10] S. Rusponi, G. Costanini, F.B. de Mongeot, C. Boragno, U. Valbusa, Appl. Phys. Lett. 75 (1999) 3318.
[11] J. Erlebacher, M.J. Aziz, E. Chason, M.B. Sinclair, J.A. Floro, Phys. Rev. Lett. 82 (1999) 2330.
[12] F. Frost, A. Schindler, F. Bigl, Phys. Rev. Lett. 85 (2000) 4116.
[13] R. Gago, L. Vázquez, R. Cuerno, M. Varela, C. Ballesteros, J.M. Albella, Appl. Phys. Lett. 78 (2001) 3316.
[14] S. Habenicht, Phys. Rev. B 63 (2001) 125419.
[15] M. Kalff, G. Comsa, T. Michely, Surf. Sci. 488 (2001) 346.
[16] M. Lu, X.J. Yang, S.S. Perry, J.W. Rabalais, Appl. Phys. Lett. 80 (2002) 2096.
[17] U. Valbusa, C. Boragno, F.B. de Mongeot, J. Phys.: Condens. Matter 14 (2002) 8153, and references therein.
[18] J. Kim, D.G. Cahill, R.S. Averback, Phys. Rev. B 67 (2003) 045404.
[19] S. Facsko, T. Bobek, A. Stahl, H. Kurz, T. Dekorsy, Phys. Rev. B 69 (2004) 153412.
[20] M. Xu, C. Teichert, J. Appl. Phys. 96 (2004) 2244.
[21] L. Ling, W.Q. Li, L.J. Qi, M. Lu, X. Yang, C.X. Gu, Phys. Rev. B 71 (2005) 155329.
[22] W.B. Fan, W.Q. Li, L.J. Qi, H.T. Sun, J. Luo, Y.Y. Zhao, M. Lu, Nanotechnology 16 (2005) 1526.
[23] B. Kahng, H. Jeong, A.-L. Barabási, Appl. Phys. Lett. 78 (2001) 805.
[24] R.M. Bradley, J.M.E. Harper, J. Vac. Sci. Technol. A 6 (1988) 2390.
[25] S. Rusponi, G. Costantini, C. Boragno, U. Valbusa, Phys. Rev. Lett. 81 (1998) 4184.
[26] S. Park, B. Kahng, H. Jeong, A.-L. Barabási, Phys. Rev. Lett. 83 (1999) 3486.
[27] G. Ehrlich, F.G. Hudda, J. Chem. Phys. 44 (1966) 1039;
R.L. Schwoebel, E.J. Shipsey, J. Appl. Phys. 37 (1966) 3682.
[28] P. Politi, J. Villian, Phys. Rev. B 54 (1996) 5114.
[29] J.P. de Souza, C.A. Cima, P.F.P. Fichtner, H. Boudinov, J. Appl. Phys. 95 (2004) 877.
[30] C. Schelling, G. Springholz, F. Schäffler, Phys. Rev. Lett. 83 (1999) 995.
[31] G. Costantini, F.B. de Mongeot, C. Boragno, U. Valbusa, Phys. Rev. Lett. 86 (2001) 838.
[32] J.F. Ziegler (Ed.), The Stopping and Range of Ions in Solids, Pergamon, New York, 1996.